It is found that the model gives good results even if D/λ_0 becomes very small. Moreover, a beam angle of 17° is achieved with a strong coupling of –7.7dB ($\Delta F/F$ = –0.002 and $\Delta F = F-F_1$ where F_1 is the resonant frequency of the lateral patch). This coupling value corresponds to a gap distance D of 0.0033 free-space wavelength (100μm) between the patch edges.

Because of H-plane coupling, the coupling mechanism is due to the space waves and not to the surface waves in the substrate. It results in a weaker mismatch of the active antenna input impedance than for E-plane coupling. When D/λ_0 increases (above 0.1), the radiation pattern exhibits an important sidelobe. D/λ_0 = 0.61 corresponds to the radiation of two major sidelobes. When D/λ_0 becomes > 1, the influence and the radiated power of the lateral patches are less significant, and the radiation pattern is that of the central patch.

For D/λ_0 = 0.0033, the main beam radiation can be tilted up to 23° from the broadside direction by adjusting the resonant frequency of the lateral patch, as shown in Fig. 3.

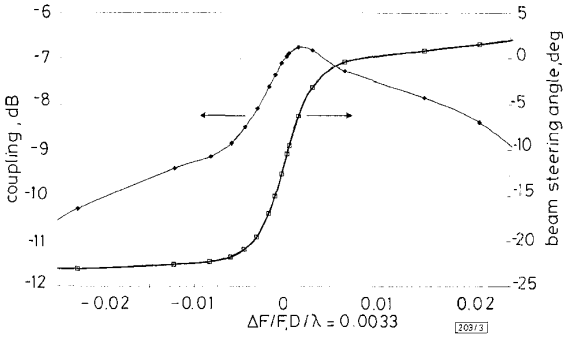

Fig. 3 *Theoretical mutual coupling coefficient and beam steering angle against difference of resonant frequencies of patches*

The beam is steered from 0 to –17° without notable degradation of radiated characteristics, as presented in Fig. 4.

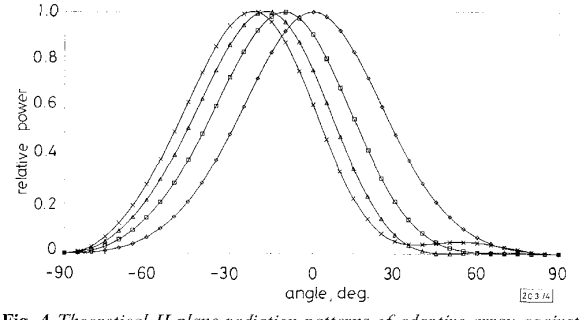

Fig. 4 *Theoretical H-plane radiation patterns of adaptive array against difference of resonant frequencies of patches*

◇ 7.5V, □ 17.5V, △ 20V, × 30V

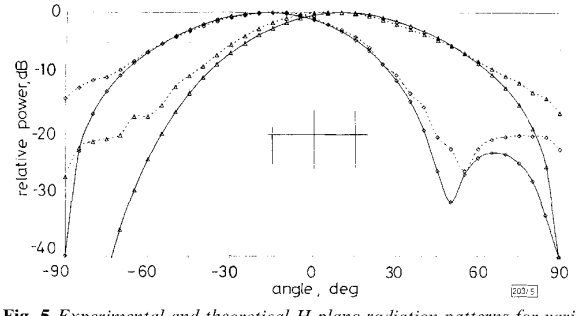

Fig. 5 *Experimental and theoretical H-plane radiation patterns for various couplings*

Theory: —◇— 0–20, —△— 17.5–0
Experiment: – –◇– – 0–20, – –△– – 17.5–0

Notice that the E-plane pattern is not affected by the coupling, as we expected.

In Fig. 5 we present the experimental and theoretical H-plane radiation patterns for two different couplings. In the first case (0–20), the radiation is due principally to the central and right patches. A high bias voltage of 20V is applied to the right patch varactor diode while the left patch varactor is at 0V bias polarisation corresponding to the decoupling of the left patch with the central patch. The measurements are in good agreement with the computed results.

In the second case (17.5–0), the main beam is more weakly steered to the opposite direction by changing the bias polarisations.

Conclusion: A well formed scannable beam is obtained from the adaptive array of three patch antennas. A beam scanning of ±15° from the broadside direction can be achieved with this configuration. A beam including a high sidelobe level is formed for larger scanning angles up to ±25°. Moreover, this technique is well suited to a monolithic integration. The low directivity of a three element patch array can be also increased by overlaying each patch with a dielectric sphere [8].

26 April 1996
Electronics Letters Online No: 19960867

D. Cailleu, N. Haese and P.A. Rolland (*Institut d'Electronique et de Microélectronique du Nord (IEMN), Domaine Scientifique et Universitaire de Villeneuve d'Ascq, Avenue Poincaré - B.P. 69, 59 652 Villeneuve d'Ascq Cedex, France*)

References

1 DINGER, R.J.: 'Reactively steered adaptive array using microstrip patch elements at 4GHz', *IEEE Trans. Antennas Propag.*, 1984, **AP-32**, (8), pp. 848–856
2 DINGER, R.J.: 'A planar version of a 4.0GHz reactively steered adaptive array', *IEEE Trans. Antennas Propag.*, 1986, **AP-34**, (3), pp. 427–431
3 BHATTACHARYYA, A.K., and GARG, R.: 'Generalised transmission line model for microstrip patches', *IEE Proc. H. Microw. Opt. Antennas*, 1985, **132**, (2), pp. 93–98
4 BHATTACHARYYA, A.K., and GARG, R.: 'Input impedance of annular ring microstrip antenna using circuit theory approach', *IEEE Trans. Antennas Propag.*, 1985, **AP-33**, (4), pp. 369–374
5 CHIH-YU HUANG, and KIN-LU WONG: 'Mutual coupling computation of probe-fed circular microstrip antennas', *Microw. Opt. Technol. Lett.*, 1995, **9**, (2), pp. 100–102
6 BHATTACHARYYA, A.K., and GARG, R.: 'Spectral domain analysis of wall admittances for circular and annular microstrip patches and the effect of surface waves', *IEEE Trans.*, 1985, **AP-33**, (10), pp. 1067–1073
7 BHATTACHARYYA, A.K., and SHAFAI, L.: 'Surface wave coupling between circular patch antennas', *Electron. Lett.*, 1986, **22**, (22), pp. 1198–1200
8 JAMES, J.R., HALL, C.M., and ANDRASIC, G.: 'Microstrip elements and arrays with spherical dielectric overlays', *IEE Proc. H. Microw. Antennas Propag.*, 1986, **133**, (6), pp. 474–482

Short leaky-wave antennas of sum and difference patterns

J.-M. Lin, C.-K.C. Tzuang, G.-J. Chou and S. Su

Indexing terms: Leaky wave antennas, Antennas

A set of differential feed short (~0.7 λ_0) leaky-wave antennas with sum (Σ) and difference (Δ) patterns is presented. Rigorous field-theory analyses show that the radiation characteristics of these antennas agree well with the measurements. The performance of these antennas is well suited for direction finding applications.

Introduction: Traditionally, the microwave passive direction finding system uses hybrid-fed networks producing sum-and-difference outputs to establish broadside (Σ) and split-beam (Δ) radiation patterns [1]. This Letter, however, presents an alternative approach to achieve Σ-Δ radiation patterns using a class of short

leaky-wave antennas with coaxial-to-microstrip transitions on which the differential signals propagate. The proposed leaky-wave antennas constitute the front-end portion of the active integrated antennas [2] as a compact and miniaturised direction finding system. In contrast to most leaky-wave antennas of moderate length from 3 to 10 λ_0, a short microstrip leaky-wave antenna of ~0.7 λ_0 long is chosen for our particular design.

The design and principle of the operation of microstrip leaky-wave antennas has been investigated thoroughly in the past by W. Menzel [3] and A.A. Oliner [4]. The micro strip's first high order mode will radiate in the form of a fan beam at $\theta_m = \sin^{-1}(\beta/k_0)$ measured from broadside below a cutoff frequency when the so called leaky-mode is excited. β is the phase constant of the leaky-mode.

When the leaky-wave antenna is short and excited from one end, with proper design, plenty of electromagnetic energy of the leaky-mode will survive when it travels down to the other end of the antenna. The remaining energy reflects backward, creating a difference pattern. When the leaky-wave antenna is centre-fed, the resultant radiation pattern appears to be the vector sum of the even-symmetric patterns generated by the equally split electromagnetic energy. Thus a broadside radiation pattern must stem from the centre-fed antenna.

Antenna designs: a and *b* of Fig. 1 illustrate schematically how the end-fed and centre-fed Ku-band microstrip leaky-wave antennas are prototyped to produce the desired Σ and Δ radiation patterns, respectively.

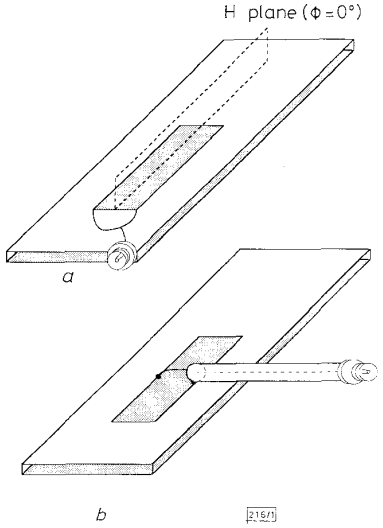

Fig. 1 *Close-up view of end-fed and centre-fed leaky-mode antennas with height = 0.635mm, width = 3.5mm, length = 18mm and εr = 10.2*

a End-fed, *b* Centre-fed

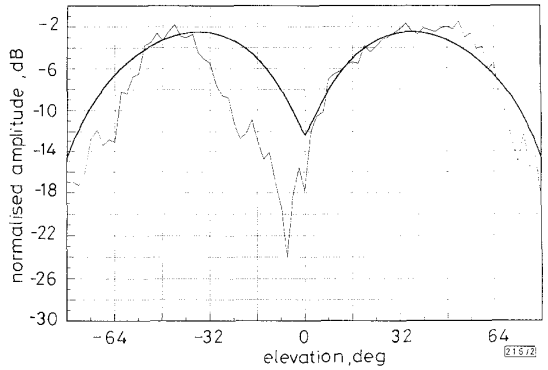

Fig. 2 *Theoretical and measured H-plane radiation patterns of microstrip leaky-mode antenna against elevation angle for end-fed coaxial-to-microstrip differential signal input*

—— theoretical, —— measured

An 18mm long and 3.5mm wide microstrip resides on top of a 25mil thick RT/Duroid 6010 substrate with relative permitivity of 10.2. In Fig. 1*a*, the centre conductor of the coaxial cable is connected to the hybrid divider that generates out-of-phase signals fed into the two ends of the microstrip. The outer conductor of the coaxial cable is connected to the ground plane of the microstrip. In the case of the centre-fed antenna in Fig. 1*b*, the centre and outer conductors of the coaxial cable are separately soldered to the opposite sides in the middle of microstrip. In both cases the coaxial-to-microstrip out-of-phase signals are present at the antenna-feeds.

Measurement and theoretical results: Planar near-field measurements of the two antenna prototypes are conducted at 12.3GHz. The microstrip is operated at the first higher order odd mode, which is a leaky-mode and can be excited by the differential signals. We observe that two peaks occur at ~ϕ (azimuth) $\simeq 0°$ and θ (elevations) $\simeq \pm 48°$ in the radiation contour plot of the end-fed antenna with maximum directivity of 13dBi. For the centre-fed antenna, one peak occurs at ~ $\phi \simeq 0°$, $\theta \simeq \pm 0°$, with maximum directivity of 11dBi. Figs. 2 and 3 show the measured radiation patterns of the end-fed and centre-fed leaky-wave antennas at the H plane ($\phi = 0°$), respectively. The ratio of the maximum peak to the null is ~23dB as shown in Fig.2, which is adequate for many direction finding applications. The null position is not at the centre of microstrip, rather at $\theta \simeq -7°$. Also shown in Fig. 2 is the theoretical result of the same antenna by application of the full-wave integral equation method [5]. Very good agreement between measurement and theory is obtained. Further numerical studies show that the null position can be adjusted by slight modification of the antenna length. Fig. 3 also shows that the theoretical and measured results agree well. The radiation pattern is indeed pointing to the broadside, as expected.

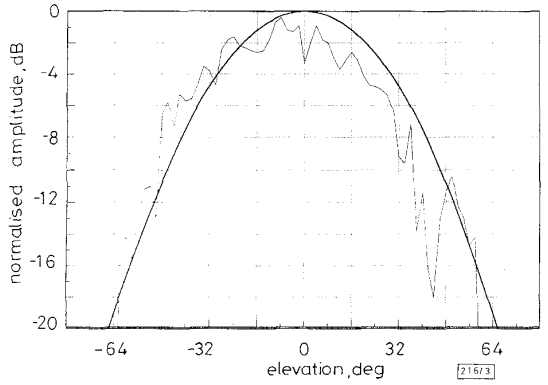

Fig. 3 *Theoretical and measured H-plane radiation patterns of microstrip leaky-mode antenna against elevation angle for centre-fed coaxial-to-microstrip differential signal input*

—— theoretical, —— measured

Conclusion: A novel set of short microstrip leaky-wave antennas is presented. While good agreement between theoretical and measured results is obtained for the antennas of sum and difference patterns, these high performance antennas can be useflil for relatively narrow-band microwave passive direction finding applications. Although the probe-fed versions of the short leaky-wave antennas are reported as quickly designed prototypes, other quasi-planar feeds can be developed and optimised for practical design.

Acknowledgment: This work was supported by the National Science Council, Taiwan, under Grant NSC 84-2623-D-009-006 and NSC 84-2623-D-009-008.

29 April 1996

Electronics Letters Online No: 19960866

J.-M. Lin, C.-K.C. Tzuang, G.-J. Chou and S. Su (*Institute of Electrical Communication Engineering, National Chiao Tung University, No. 1001, Ta Hsueh Road, Hsinchu, Taiwan, Republic of China*)

References

1 LIPSKY, S.E.: 'Microwave passive direction finding' (John Wiley & Sons, New York, 1987)
2 JENSHAN-LIN, and ITOH, T.: 'Active integrated antenna', *IEEE Trans. Microw. Theory Tech.*, 1994, **MTT-42**, (12), pp. 2186–2194
3 MENZEL, W.: 'A new traveling-wave antenna in microstrip'. AEÜ 33, April 1979, pp. 37–140
4 OLINER, A.A., and LEE, K.S.: 'Microstrip leaky wave strip antennas'. IEEE Int. Antennas Propag. Symp. Dig., 1986, **1**, pp. 443–446
5 LO, W.T., TZUANG, C.K.C., PENG, S.T., TIEN, C.C., CHUNG-CHI CHANG, and JENQ-WEN HUANG: 'Resonant phenomena in conductor-backed coplanar waveguides (CBCPWs)', *IEEE Trans. Microw. Theory Tech.*, 1993, **MTT-41**, pp. 2099–2108

CMOS parametric current amplifier

R. Fried and C.C. Enz

Indexing terms: Parametric amplifiers, CMOS integrated circuits, Current-mode circuits

The current amplifier presented is based on a gate-bulk-source translinear loop of MOSTs biased in weak inversion. Large gain factors are achieved with the consumption of only a small area. Gain is controlled by a ratio of bias currents.

Introduction: Current amplification in CMOS is traditionally carried out by static and dynamic current mirrors, or operational transconductance amplifiers (OTA) [1]. These circuits consume a large area when large controlled gain is needed. The current amplifier presented here is based on a MOST translinear loop [2, 3]. Its high efficiency is due to the fact that it takes advantage of all degrees of freedom of a MOST biased in weak inversion and in saturation, i.e. the aspect ratio, and the gate-to-source and bulk-to-source voltages. Its gain factor is adjusted by bias currents and thus it is especially suitable for current-mode automatic gain control (AGC) circuits.

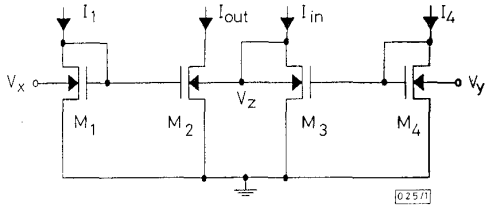

Fig. 1 *Basic principle of current amplifier*

Basic principle: The drain current of a MOST, biased in weak inversion and in saturation is given by [4]:

$$I_D = I_{D0}\exp\left(\frac{V_{GS}}{nU_T}\right)\exp\left(\frac{n-1}{n}\frac{V_{BS}}{U_T}\right)$$

$$I_{D0} \propto (W/L) \qquad (1)$$

where I_{D0} is the leakage current (when $V_{GS} = V_{BS} = 0$), n is the slope factor and $U_T = (kT)/q$ is the thermodynamic voltage. The amplifier basic principle is shown in Fig. 1 where all the MOSTs are assumed to be biased in weak inversion and in saturation. Assuming that all the MOSTs have the same slope factor n, the input and output currents, I_{in} and I_{out} respectively, are given by:

$$I_{in} = I_4\frac{I_{D0_3}}{I_{D0_4}}\exp\left(\frac{n-1}{n}\frac{V_z - V_y}{U_T}\right) \qquad (2)$$

$$I_{out} = I_1\frac{I_{D0_2}}{I_{D0_1}}\exp\left(\frac{n-1}{n}\frac{V_z - V_x}{U_T}\right) \qquad (3)$$

Dividing the two equations yields:

$$I_{out} = I_{in}\underbrace{\frac{I_{D0_2}I_{D0_4}}{I_{D0_1}I_{D0_3}}}_{K_1}\underbrace{\frac{I_1}{I_4}}_{K_2}\underbrace{\exp\left(\frac{n-1}{n}\frac{V_y - V_x}{U_T}\right)}_{K_3} = KI_{in} \qquad (4)$$

According to eqn. 4, the gain can be controlled by three parameters: the transistors' aspect ratios via the I_{D0}s (classical method) – K_1, the ratio between the two bias currents I_1 and I_4 – K_2, and the difference between the two bulk bias voltages V_x and V_y – K_3. The latter can also be realised as a ratio between two bias currents, as will be shown later. Eqn. 4 indicates that large gain factors are achievable with the consumption of a small area. In addition, the gain factor can be easily adjusted via bias currents.

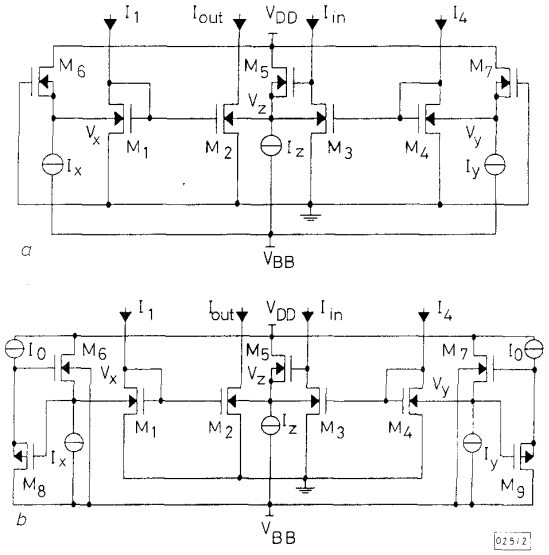

Fig. 2 *Parametric current amplifier*

a With gate driven source followers
b With bulk driven source followers

Current amplifier: A complete current-mode configuration of the current amplifier is shown in Fig. 2. The voltage follower M_5 was added to maintain M_3 in saturation, and prevent the bulk-to-source junctions of M_2 and M_3 from being forward biased. The difference between the bulk bias voltages V_y and V_x is generated by the ratio between the bias currents I_x and I_y, of the gate driven source followers M_6 and M_7 in Fig. 2*a*, and the bulk driven source followers in Fig. 2*b*. When using bulk driven source followers, a more efficient gain factor is achieved at the expense of additional components (and current consumption) necesary to bias the gate-to-source junctions of M_6 and M_7. The relation between the output and input currents is given by:

$$I_{out} = I_{in}\frac{I_1}{I_4}\left(\frac{I_x}{I_y}\right)^{\alpha} \qquad (5)$$

where $\alpha = n$–1 for the gate driven source followers, and $\alpha = 1$ when bulk driven source followers are used. It is assumed in eqn. 5 that $K_1 = 1$. The additional supply voltage V_{BB} is used to assure negative bulk-to-source voltages for all the MOSTs in the circuit. The necessary rail-to-rail voltage ($V_{DD} - V_{BB}$) is only 1V, since there are no paths with more than one threshold voltage drop. Assuming $I_4 = I_y = I_z$, and that the input quiescent current is also biased at the same level, the output current noise spectral density is given by:

$$\begin{aligned} S_{out} &= S_2 + (K_2K_3)^2(S_3 + S_4 + S_5 + S_7) \\ &\quad + K_2^2(n_1 - 1)^2S_6 + K_2^2S_1 \\ &\simeq S_2 + 4K^2S_3 \end{aligned} \qquad (6)$$

where S_i is the noise current spectral density of transistor i. This result is equivalent to the case of a classical current mirror with a gain equal to $2K$. Since large gain factors are achieved without requiring large transistor size ratios, small devices may be used in order to reduce parasitic capacitance. In this case the amplifier bandwidth depends only on the load capacitance and the level of the output current. In addition, it has a low input capacitance, unlike traditional current mirrors with large current gain.